

Phase Transition and Diffusion in an Adiabatic Bouncer Model

Luiz Antonio Barreiro^{1,*}

¹*Institute of Geosciences and Exact Sciences,
Physics Department, São Paulo State University (Unesp),
CEP 13506-900, Rio Claro, São Paulo, Brazil*

This study examines anomalous diffusion and dynamical phase transitions in a nonlinear bouncer model with short-range interactions leading to velocity-dependent (adiabatic) collisions. By varying a control parameter, transitions between superdiffusion, normal diffusion, subdiffusion, and complete dynamical freezing are observed. The phase behavior is characterized via scaling laws and critical exponents, providing a robust framework for understanding the underlying dynamics.

Introduction - Nonlinear dynamical systems display a wide range of complex behaviors, including bifurcations, chaos, anomalous diffusion, and phase transitions [1, 2]. Among these, transport phenomena such as diffusion often deviate from classical Brownian motion when governed by nonlinear or chaotic dynamics. In such cases, deterministic chaos and nonlinearity can lead to anomalous diffusion, where the mean square displacement scales as $\langle x^2(t) \rangle \sim t^\mu$ with $\mu \neq 1$ [3, 4].

Dynamical phase transitions—abrupt changes in statistical behavior driven by control parameters—are marked by shifts in the scaling exponent μ , indicating regimes of superdiffusion ($\mu > 1$), normal diffusion ($\mu = 1$), subdiffusion ($\mu < 1$), or complete suppression of transport (freezing) [5, 6].

Models such as bouncers [7, 8], kicked rotators [9], and nonlinear maps [10] have been widely used to study how phase space structure influences diffusion and critical behavior.

This work investigates a modified bouncer model incorporating an adiabatic parameter that accounts for molecular-scale interactions during collisions. The classical bouncer model—describing a particle colliding elastically with an oscillating surface under gravity—serves as a key system for studying Fermi acceleration and chaotic transport. Introducing velocity-dependent restitution or finite-time interactions extends the model’s physical relevance, allowing for the analysis of anomalous transport, transitions to a frozen regime, and critical phenomena. Emphasis is placed on scaling laws and critical exponents that characterize the system near the transition point.

Collision process - The analysis begins with the classical bouncer model, which describes a particle subject to a uniform gravitational field g , undergoing successive collisions with a platform that oscillates harmonically in time. In the reference frame of the oscillating surface, the velocity of the particle relative to the platform at the instant of collision is expressed as $v'_i = v_i - V$, where v_i is the particle’s velocity just before the collision in the lab frame, and V is the instantaneous velocity of the surface. Assuming elastic collisions ($v'_f = -v'_i$) and transforming back to the laboratory frame, we obtain

$$v_f = |v_i| + 2V. \quad (1)$$

To improve the physical realism of the bouncer model, molecular-scale effects can be included by accounting for short-range repulsive forces, such as dipole interactions [11]. Unlike idealized instantaneous collisions, the interaction occurs over a finite time $\tau \sim \ell/v_n$, where ℓ is a characteristic interaction length and v_n the particle’s incident velocity. During this interval, the wall’s velocity is effectively time-averaged over the contact duration τ , yielding

$$\langle V \rangle = \frac{1}{\tau} \int_{t_c}^{t_c+\tau} \zeta \omega \cos(\omega t) dt \approx \zeta \omega \left[\cos(\omega t_c) - \frac{\omega \ell}{2v_i} \sin(\omega t_c) \right], \quad (2)$$

where t_c is the collision time, and ζ , ω characterize the amplitude and frequency of the wall’s motion. The first term represents the instantaneous velocity of the wall, while the second accounts for the time-dependent force during contact.

This finite-time correction becomes especially relevant for slow-moving particles ($v_i \ll 1$), introducing significant deviations from elastic behavior. For fast particles ($v_i \gg 1$), the interaction becomes effectively instantaneous, recovering the adiabatic limit.

The Map - Based on the Eqs (1) and (2), we construct a discrete map describing the velocity update after each collision. At the $(n + 1)$ -th bounce, the particle velocity is given by

$$v_{n+1} = \left| \left[1 + \frac{\zeta \sin(\omega t_{n+1})}{v_n^z} \right] v_n \right|, \quad (3)$$

where the z parameter controls the degree of adiabaticity. For $z = 1$, the interaction mimics instantaneous contact; for $z = 2$, it models a finite-duration force response. The modulus dictates that a particle with negative velocity is absorbed by the surface, and a new particle is injected with equal magnitude but opposite velocity.

Between collisions, the particle undergoes free fall in a uniform gravitational field. The time between bounces is $t_{n+1} - t_n = \frac{2v_n}{g}$. Introducing the dimensionless variables $\phi_n = \omega t_n$ and $V_n = \omega v_n/g$, the dynamics is governed by the two-dimensional map

$$\begin{aligned} \phi_{n+1} &= \phi_n + 2V_n, \\ V_{n+1} &= \left| V_n + \frac{\bar{\zeta}}{V_n^{z-1}} \sin(\phi_{n+1}) \right|, \end{aligned} \quad (4)$$

where an effective parameter $\bar{\zeta} = \zeta(\omega/g)^z$ was defined. This map captures the transition from chaotic diffusion to localized dynamics, depending on the choice of z and $\bar{\zeta}$.

Diffusion Process - It is possible to use an analytical argument to predict the unlimited diffusion of energy through the Fermi acceleration mechanism [12]. Let us consider an ensemble of particles with initially low velocities, which means an ensemble characterized by a low temperature, but sufficiently high to neglect quantum effects. Squaring the second equation in mapping (4), and making an ensemble average over $\phi \in [0, 2\pi]$, yields

$$\langle V_{n+1}^2 \rangle = \langle V_n^2 \rangle + \frac{1}{2} \bar{\zeta}^2 \langle V_n^{2-2z} \rangle. \quad (5)$$

In the asymptotic limit of large n , the relationship can be expressed as

$$\frac{\partial \langle V_n^2 \rangle}{\partial n} \simeq \frac{\langle V_{n+1}^2 \rangle - \langle V_n^2 \rangle}{(n+1) - n} = \frac{\bar{\zeta}^2}{2} \langle V_n^{2-2z} \rangle. \quad (6)$$

To advance further, let us assume a Gaussian form for the distribution, with an anomalous diffusion $\Psi_\mu(V, n) = \sqrt{\frac{a}{\pi}} \frac{1}{n^\mu} e^{-a(\frac{V}{n^\mu})^2}$ [13, 14]. Under this assumption, it is possible to write $\langle V_n^{2-2z} \rangle = \int_{-\infty}^{\infty} V^{2-2z} \Psi_\mu(V, n) dV = \frac{2^{1-z}}{\sqrt{\pi}} \Gamma(\frac{3}{2} - z) \langle V_n^2 \rangle^{1-z}$ leading to a differential equation in $\langle V_n^2 \rangle$. The solution to this equation can then be expressed as

$$\langle V_n^2 \rangle = \left\{ V_0^{2z} + z \Gamma\left(\frac{3}{2} - z\right) \frac{\bar{\zeta}^2}{\sqrt{\pi}} n \right\}^{1/z} \sim (\beta n)^{1/z}. \quad (7)$$

where we have defined $\beta(z, \bar{\zeta}) = z \Gamma(\frac{3}{2} - z) \frac{\bar{\zeta}^2}{\sqrt{\pi}}$ and V_0 is the initial velocity.

The results presented in (7) demonstrate that the diffusion behavior of the system is critically dependent on the value of the adiabatic parameter. In this context, normal diffusion corresponds to a mean square velocity (MSV) that grows linearly with the number of iterations n ($z = 1$). Superdiffusion is characterized by an MSV that increases faster than linearly with n ($z < 1$), typically associated with long-range correlations or persistent motion. Conversely, subdiffusion is identified by an MSV that grows more slowly than linearly, often resulting from dynamical trapping or stability effects in phase space ($z > 1$). Thus, the z parameter functions as a critical control parameter, governing the transition between superdiffusive, diffusive, and subdiffusive regimes in the system's energy transport. This parameter effectively modulates the rate and nature of energy transfer within the system, influencing the overall dynamic behavior and allowing for precise manipulation of diffusion processes.

Trapping Criterion at Low Velocity - The derivation of these diffusion regimes relies on two principal assumptions: The phase variable ϕ is uncorrelated and uniformly distributed and the motion persists indefinitely,

without interruption. Nevertheless, these assumptions break down in the regime where $z \ll 1$. In this limit, the perturbative term

$$\frac{\bar{\zeta}}{V_n^{z-1}} \sin(\phi_{n+1}) \approx \bar{\zeta} V_n [1 - z \ln(V_n)] \sin(\phi_{n+1}) \quad (8)$$

tends to vanish as $V_n \rightarrow 0$, introducing a nonlinear suppression of motion at low velocities. This suppression is particularly significant when $\phi_n \approx 0 \pmod{\pi}$, where $\sin(\phi_{n+1}) \approx 0$, further inhibiting the system's ability to sustain motion. As a result, the system may become trapped in a dynamically frozen state. This behavior signals the occurrence of a dynamical phase transition into a frozen regime when the adiabatic parameter falls below a critical threshold $z_c(\bar{\zeta})$, even though naive scaling arguments would predict an enhancement of superdiffusion for $z < 1$.

Under the condition that $\phi_n \approx 0 \pmod{\pi}$, the trapping condition can thus be expressed by examining the magnitude of the velocity increment in the map equations (4):

$$|V_{n+1} - V_n| = |\Delta V| \approx V_n^{1-z} \bar{\zeta} \eta, \quad (9)$$

where we have defined $\eta = \sin(\phi_{n+1}) \ll 1$. This relation indicates that, under these circumstances, the perturbation is insufficient to significantly alter the velocity, causing the orbit to remain trapped near V_n .

To estimate the minimum perturbation ΔV_{\min} necessary for escape from the trapping region, we require: $\Delta V_{\min} \gtrsim V_n$, leading to the condition

$$\bar{\zeta} \eta \gtrsim V_n^z. \quad (10)$$

Solving for z , we obtain the critical trapping threshold:

$$z \lesssim z_c(\bar{\zeta}) \approx \frac{\ln(\eta \bar{\zeta})}{\ln(V_n)} \approx \frac{\ln(\eta)}{\ln(V_n)} + \frac{\ln(\bar{\zeta})}{\ln(V_n)}. \quad (11)$$

where it is taken into account that, from a numerical standpoint, both η and V are small, on the order of 10^{-3} , and can be adjusted in accordance with numerical simulations.

This modified bouncer map is formally a twist map, because $\frac{\partial \phi_{n+1}}{\partial V_n} = 2$ for all (ϕ_n, V_n) , but it dynamically behaves as a non-twist map in the low-velocity (freezing) regime. The effective rotation number, $\Omega(V_n) = 2 \langle V_n \rangle$, approaches zero in the freezing phase ($z < z_c(\bar{\zeta})$), becoming flat across initial conditions and leading to $\frac{d\Omega}{dV} \rightarrow 0$. This behavior characterizes non-twist maps, known for supporting shearless barriers, reconnection zones, and enhanced stickiness.

Numerical Analysis - To substantiate the theoretically predicted dynamical behaviors, extensive numerical simulations were performed, consisting of $n = 10^6$ iterations for each of 10^4 distinct initial conditions. The choice of $n = 10^6$ ensures that the long-term behavior of the system is accurately captured, while the use of 10^4 distinct

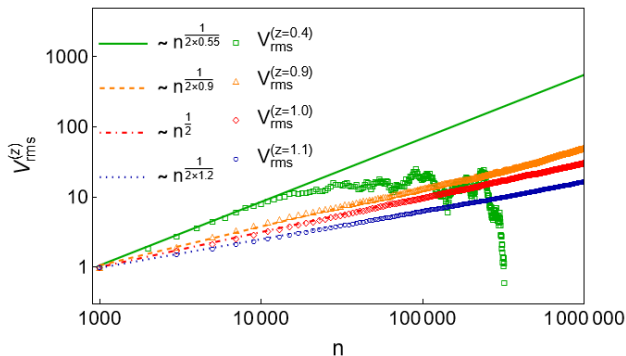


Figure 1. Plots of V_{rms} for four values of z are shown, based on an ensemble of 10^4 initial conditions uniformly distributed in $\phi \in [0, 2\pi]$ and evolved over 10^6 iterations. To enable meaningful comparison across diffusive regimes, all curves are normalized such that $V_{\text{rms}}^{(z)}(1000) = 1$. Simulations use $\bar{\zeta} = 5$ with $z = 1.1, 1.0, 0.9$, and 0.429 . Solid (green), dashed (orange), dot-dashed (red), and dotted (blue) lines represent the theoretical predictions from Eq. (7).

initial conditions mitigates the influence of specific trajectories. The observable under consideration is the root-mean-square velocity, computed over an ensemble of M initial conditions and defined as $V_{\text{rms}}^{(z)}(n) = \sqrt{\langle V_n^2 \rangle} = \sqrt{\frac{1}{M} \sum_{i=1}^M V_{i,n}^2}$. These simulations were conducted for four representative values of the z parameter: namely, $z = 1.1$, $z = 1.0$, $z = 0.9$, and $z = 0.4$, with $\bar{\zeta} = 5$, where the invariant curves have already been eliminated [15]. According to Eq. (7), the expected asymptotic behaviors for the observable are as follows: for $z = 1.1$, the growth follows $\sim n^{1/2.2}$; for $z = 1.0$, $\sim n^{1/2}$; for $z = 0.9$, $\sim n^{1/1.8}$; and for $z = 0.4$, $\sim n^{1/0.8}$.

Figure 1 displays the numerical results corresponding to the cases $z = 1.1$, $z = 1.0$, and $z = 0.9$, which demonstrate good agreement with the theoretical predictions. The observed behavior corroborates the expected scaling laws, thereby validating the analytical framework presented. For $z = 0.4$, the root-mean-square velocity initially displays superdiffusive growth, approximately following the predicted power law. However, beyond $n \gtrsim 10^5$, $V_{\text{rms}}^{(z)}$ undergoes a rapid decline towards zero, indicating the onset of a dissipative mechanism that drives the system into a dynamically frozen state. This transition to a frozen state is analogous to a sublimation process.

Eq. (11) predicts a transition to a dynamically frozen state when the adiabatic z parameter drops below a critical threshold. This is confirmed numerically for $z = 0.4$ and $\bar{\zeta} = 5$, as shown in figure 1. To further investigate this transition, we construct a “phase” diagram that elucidates the dependence of the system’s dynamical behavior on the parameters $\bar{\zeta}$ and z .

This analysis involves generating a two-dimensional grid of discrete parameter values, with $\bar{\zeta}$ ranging from

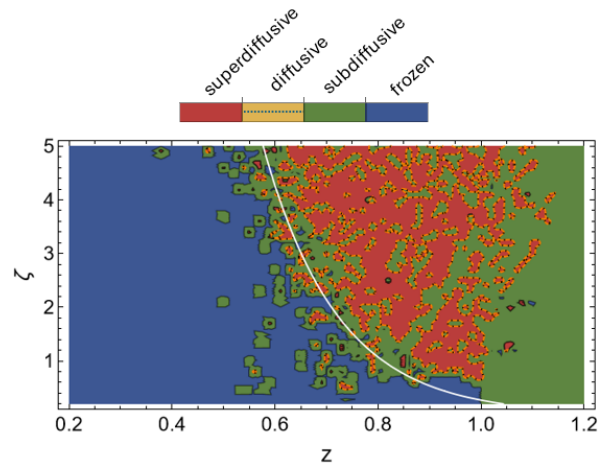


Figure 2. The phase diagram is categorized by the power-law relation $V_{\text{rms}} = an^b$. Subdiffusion occurs for $b \leq 0.49$, superdiffusion for $b \geq 0.51$, and normal diffusion is identified in the intermediate range $0.49 < b < 0.51$, marked by a dotted boundary. The white line indicates the theoretical prediction from Eq. (11) with $\eta = 0.0037$ and $V_n = 0.001$.

0.2 to 5.0 and z spanning the interval from 0.2 to 1.2. For each pair $(\bar{\zeta}, z)$ in this grid, we compute the corresponding root-mean-square velocity $V_{\text{rms}}^{(z)}$. Eq. (7) shows that V_{rms} evolves as a power-law function of the number of iterations n , i.e., $V_{\text{rms}} = an^b$, where a is a constant and b is the diffusion exponent characterizing the system’s long-term behavior.

The exponent b serves as a diagnostic for classifying the diffusion regime. Specifically, for $b \leq 0.49$, the system exhibits subdiffusive behavior, characterized by dispersion slower than that of normal diffusion. In the range $0.49 < b < 0.51$, the diffusion is approximately normal, implying a linear growth of mean-square velocity with time. Finally, for $b \geq 0.51$, the system enters the superdiffusive regime, where the transport process is faster than in the normal diffusive case.

These classifications and their corresponding behaviors are illustrated in the accompanying figure 2, which visually represents the varying diffusion regimes as a function of the parameters $\bar{\zeta}$ and z . Given that normal diffusive behavior is confined to a narrow range of b values, it is represented by dashed lines at the boundaries between subdiffusive (green region) and superdiffusive regimes (red region). The blue region represents the frozen phase. The white curve in the figure corresponds to the theoretical relationship

$$z_c = 0.86 - 0.217 \ln(\bar{\zeta}), \quad (12)$$

as given by Eq. (11). This expression was obtained using the parameter values $\eta = 0.019$ and $V_n = 0.01$, which are consistent with the assumption that both η and V_n are small.

Naturally, this theoretical result—derived from a sim-

plified dimensional analysis—does not capture the detailed structure of the boundary. Nevertheless, it provides a remarkably good approximation of the overall trend observed in the boundary as revealed by numerical simulations showed in figure 2. It should be emphasized that once the system enters the frozen regime, increasing the number of iterations does not restore diffusive behavior. Likewise, for fixed control parameters $\bar{\zeta}$ and z , increasing the number of initial conditions—even beyond 10^4 —does not alter the macroscopic dynamical state. Both the diffusive and frozen phases thus exhibit robustness with respect to ensemble size and integration time.

The transition boundaries observed numerically are neither smooth nor sharply defined, reflecting the non-linear nature of the system, which includes fixed points and stability islands embedded in a chaotic phase space. These structures lead to abrupt dynamical changes under small variations in z and $\bar{\zeta}$, emphasizing the system's sensitivity to the parameters. To quantify the geometric complexity of the transition boundary, the Box-Counting Method [16] was employed. The frontier dimension D is estimated via the scaling relation: $D = \lim_{\epsilon \rightarrow 0} \frac{\log N(\epsilon)}{\log(1/\epsilon)}$, where ϵ is the box size and $N(\epsilon)$ is the number of boxes required to cover the boundary. The interface delimiting the normal diffusive regime exhibits a dimension of $D \approx 1.517$, revealing a nontrivial fractal geometry. This structure is consistent with critical behavior near dynamical phase transitions and reflects scale-invariant organization in phase space [10, 17, 18]. These manifestations of criticality and scale invariance serve to characterize the underlying dynamical transition to the frozen phase.

Dynamical Phase Transition - This adiabatic bouncer map exhibits a rich variety of diffusive behaviors depending on the parameters $\bar{\zeta}$ and z , especially a dynamical phase transition to a frozen state as the z parameter decreases below the critical value $z_c(\bar{\zeta})$. This transition is characterized by the vanishing of the long-term energy growth, leading to a dynamically trapped or “frozen” regime. To quantify this transition, we define the *order parameter* as the asymptotic average velocity per iteration:

$$\mathcal{V}_\infty = \lim_{n \rightarrow \infty} \ll V_n \gg, \quad (13)$$

where $\ll V_n \gg = \sqrt{\frac{\langle V_n^2 \rangle}{n}}$. This quantity is positive for $z > z_c$ and vanishes continuously as $z \rightarrow z_c^+$. The critical behavior of \mathcal{V}_∞ near the transition is captured by the scaling law:

$$\mathcal{V}_\infty \sim (z - z_c)^\beta, \quad \text{for } z \rightarrow z_c^+, \quad (14)$$

where β is the critical exponent associated with the phase transition. This is analogous to magnetization M in ferromagnetic systems. The numerical results for \mathcal{V}_∞ as a

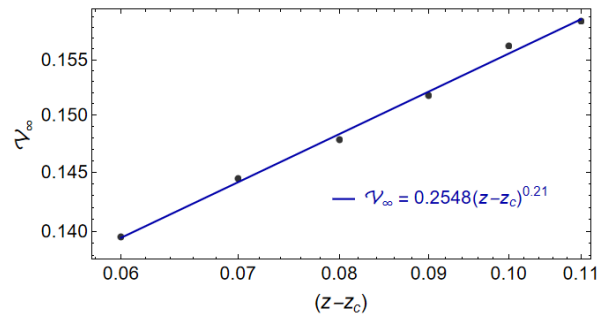


Figure 3. Log-Log Plot of \mathcal{V}_∞ by $(z - z_c)$, with $\bar{\zeta} = 5$ and $z_c = 0.55$.

function of $(z - z_c)$ with $\bar{\zeta} = 5$ and $z_c = 0.55$ are presented in Figure 3, providing support for the theoretical prediction given by Eq.(14).

The dynamical susceptibility is then defined as

$$\chi(z) \sim \frac{d}{dz} (z - z_c)^\beta = \beta (z - z_c)^{\beta-1}. \quad (15)$$

The numerical analysis yields a critical exponent $\beta = 0.21$, indicating a divergence of the dynamical susceptibility, as described by Eq. (15), in the limit $z \rightarrow z_c^+$. This behavior is characteristic of a second-order (continuous) phase transition.

Conclusions and outlook - This study demonstrates that the adiabatic parameter plays a critical role in governing both the energy exchange mechanisms and the underlying dynamical structure of the system. Variations in this parameter give rise to distinct dynamical regimes—namely, subdiffusion, normal diffusion, and superdiffusion—and culminate in a second-order phase transition from diffusive behavior to a frozen state. The presence of fractal boundaries separating these diffusive regimes highlights a pronounced sensitivity to initial conditions and parameter values, underscoring the intricate and complex organization of the system's phase space.

The twist-to-non-twist transition marks a topological change linked to the breakdown of KAM tori, enriching the system's dynamical behavior. These findings have broader relevance to systems driven by adiabatic interactions and nonlinear transport.

As a perspective for future research, the adiabatic framework developed herein may be directly extended to dynamical billiard systems with time-dependent boundaries. In particular, a connection with thermodynamic concepts—through a formal definition of entropy—offers a promising avenue for exploration, with potential implications for one- and two-dimensional gas models. Furthermore, generalizations incorporating stochastic perturbations, inter-particle interactions, or external driving forces could provide deeper insights into the robustness and universality of the dynamical phase transitions identified in this work.

Acknowledgments—The author thanks Prof. Edson Denis Leonel for his valuable contributions to this work.

* luiz.a.barreiro@unesp.br

- [1] S. H. Strogatz, *Nonlinear Dynamics and Chaos: With Applications to Physics, Biology, Chemistry, and Engineering* (CRC Press, 2018).
- [2] E. Ott, *Chaos in Dynamical Systems* (Cambridge University Press, 2002).
- [3] R. Klages, G. Radons, and I. M. Sokolov, eds., *Anomalous Transport: Foundations and Applications* (Wiley-VCH, 2008).
- [4] R. Metzler and J. Klafter, *Physics Reports* **339**, 1 (2000).
- [5] R. Venegeroles, *Physical Review Letters* **102**, 064101 (2009).
- [6] V. Zaburdaev, S. Denisov, and J. Klafter, *Reviews of Modern Physics* **87**, 483 (2015).
- [7] B. Liebchen, F. K. Diakonov, and P. Schmelcher, *New Journal of Physics* **13**, 093039 (2011).
- [8] E. D. Leonel and P. V. E. McClintock, *Journal of Physics A: Mathematical and General* **37**, 8937 (2004).
- [9] B. V. Chirikov, *Physics Reports* **52**, 263 (1979).
- [10] G. M. Zaslavsky, *Physics Reports* **371**, 461 (2002).
- [11] K. Huang, *Statistical Mechanics, 2nd Edition* (1987), URL <https://ui.adsabs.harvard.edu/abs/1987stme.book.....H>.
- [12] E. D. Leonel and A. L. P. Livorati, *Communications in Nonlinear Science and Numerical Simulations* **20**, 159 (2015), ISSN 1007-5704, 1405.2030, URL <https://ui.adsabs.harvard.edu/abs/2015CNSNS...20..159L>.
- [13] F. Ceconi, G. Costantini, A. Taloni, and A. Vulpiani, *Physical Review Research* **4**, 023192 (2022), 2206.06786, URL <https://ui.adsabs.harvard.edu/abs/2022PhRvR...4b3192C>.
- [14] A. L. Boscolo, V. B. d. S. Junior, and L. A. Barreiro, *Physical Review E* **107**, 045001 (2023), ISSN 2470-0053.
- [15] L. Miranda, C. Kuwana, Y. Huggler, and et al., *Eur. Phys. J. Spec. Top.* **231**, 167 (2022), ISSN 1951-6401.
- [16] H. Peitgen, H. Jürgens, and D. Saupe, *Chaos and fractals - new frontiers of science (2. ed.)* (Springer, 2004), ISBN 978-0-387-20229-7.
- [17] C. Grebogi, E. Ott, and J. A. Yorke, *Physical Review Letters* **50**, 935 (1983), ISSN 0031-9007.
- [18] T. Tél and Y.-C. Lai, *Physics Reports* **460**, 245 (2008), ISSN 0370-1573.